

Localized vortex beams in anisotropic Lieb lattices

Cristian Mejía-Cortés* and Jorge Castillo-Barake

Programa de Física, Facultad de Ciencias Básicas,

Universidad del Atlántico, Puerto Colombia 081007, Colombia

Mario I. Molina

Departamento de Física, Facultad de Ciencias,

Universidad de Chile, Casilla 653, Santiago, Chile

Abstract

We address the issue of nonlinear modes in a two-dimensional waveguide array, spatially distributed in the Lieb lattice geometry, and modeled by a saturable nonlinear Schrödinger equation. In particular, we analyze the existence and stability of vortex-type solutions finding localized patterns with symmetric and asymmetric profiles, ranging from topological charge $S = 1$ to $S = 3$. By taking into account the presence of anisotropy, which is inherent to experimental realization of waveguide arrays, we identify different stability behaviors according to their topological charge. Our findings might give insight on experimental feasibility to observe these kind of vortex states.

arXiv:2005.09650v1 [physics.optics] 19 May 2020

* ccmejia@googlemail.com

I. INTRODUCTION

Localized vortex beams (VBs) are interesting objects that can emerge in nonlinear optical lattices. They are characterized by several bright spots, which are spatially distributed according to the refractive index distribution, maintaining a nontrivial phase distribution in space. This phase circulates around a singular point, or central core, changing by $2\pi S$ times in each closed loop around it (with S being an integer number). The integer number S is known as the topological charge (TC) of the vortex. In general, optical vortices have been envisioned as a mean to codify information using their TC value in classical [1] and quantum [2] regimes. A stable vortex is capable of delivering angular momentum to a nearby object, hence, one of its most remarkable applications are optical tweezers in biophotonics, where they are useful due to their ability to affect the motion of living cells, virus, and molecules [3, 4]. Other applications can be found in optical systems communication [5] and spintronics [6].

Given an optical nonlinear medium of a specific geometry, we are interested in ascertaining whether vortex solitons can exist in principle and its stability properties. For homogeneous media, a self-focusing Kerr nonlinearity leads to the collapse of any two-dimensional solution [7]. Bright solitons can be stabilized by adding a transversal periodic refractive index, but, any non fundamental solution becomes unstable as they collapse upon propagation. However, recently has been shown that by inserting spatially alternating gain and losses, stable localized vortices can exist under the same nonlinear scenery [8]. On the other hand, photorefractive materials, where the linear refractive index can be modulated externally by light, vortex solitons have been envisioned theoretically [9] and observed experimentally [10] in two-dimensional square lattices at focussing regime. The nonlinear response for these crystals features a saturable nature and its limit value depends of the voltage applied to the crystal, among other parameters. Hence, photorefractive crystal becomes a terrific workbench to observe localized patterns. However, its underlying mechanism (the photorefractive effect) is intrinsically anisotropic, which for example causes deformation of the induced waveguides [11].

During the last decade, femtosecond laser inscription technique has shown solid and versatile results in fabrication of optical waveguides, both in amorphous [12] and crystalline dielectric materials [13]. In the latter case, it would be desirable to achieve nonlinear pho-

tonic lattices by direct laser writing in photorefractive materials, e. g., barium titanate (BaTiO₃), lithium niobate (LiNbO₃), strontium barium niobate (SBN), etc. In this fashion, it could be possible to tailor an unique experimental setting where a saturable nonlinearity can be combined with a strong refractive index variation, transversal to propagation axis of light. Motivated for this scenery, we aim at delving into the stability properties of such vortex solitons as supported modes of a Lieb lattice, in the presence of anisotropy, from a tight-binding approach. The choice of the Lieb lattice is interesting since it is one of several 2D lattices that display a flat band in its spectra, from which originates compacton-like states [14, 15]. In that respect, our results could give some quantitative insight, in terms of parameters of the system, about experimental observation of these kind excitations. Hence, we hope that our findings stimulate experimental realization of such photonic lattices.

II. MODEL

We start from a model of coupled optical beams in a nonlinear periodic medium. From Maxwell's equations one obtains a paraxial equation which is further approximated by a coupled-modes expansion, ending up in the discrete nonlinear Schrödinger (DNLS) equation. This model, in its general form, can be written as

$$-i \frac{dU_{\vec{n}}}{dz} = \sum_{\vec{m}} C_{\vec{n},\vec{m}} U_{\vec{m}} + F(|U_{\vec{n}}|^2) U_{\vec{n}}, \quad (1)$$

where $U_{\vec{n}}$ is the electric field amplitude at waveguide \vec{n} , z is the coordinate along the longitudinal direction, $C_{\vec{n},\vec{m}}$ are the coupling terms between sites \vec{n} and \vec{m} . The last term assume the role of nonlinear response of the system, that in our case will be modeled by the real function $F(|U_{\vec{n}}|^2) = -\gamma/(1 + |U_{\vec{n}}|^2)$, standing for a photorefractive media whose nonlinear coefficient γ is proportional to the external applied voltage.

We will use the Lieb lattice, a kind of a diluted square lattice, that corresponds to a 2D version of the perovskite structure [cf. Fig. 1 (a)], that has three sites in its unit cell (denoted by the shadow region), and a lattice constant with length equal to a . We will consider coupling to nearest-neighbors only and we introduce anisotropy by setting the horizontal coupling C_h different from the vertical one, C_v . By keeping the first term in expansion of nonlinear response, i. e., $F(|U_{\vec{n}}|^2) \approx -\gamma$, and using the Bloch functions $U_{n,m} = u_{n,m} \exp[i(k_x n + k_y m)a + i\lambda z]$ as solutions of the Eq. (1), the dispersion relation for

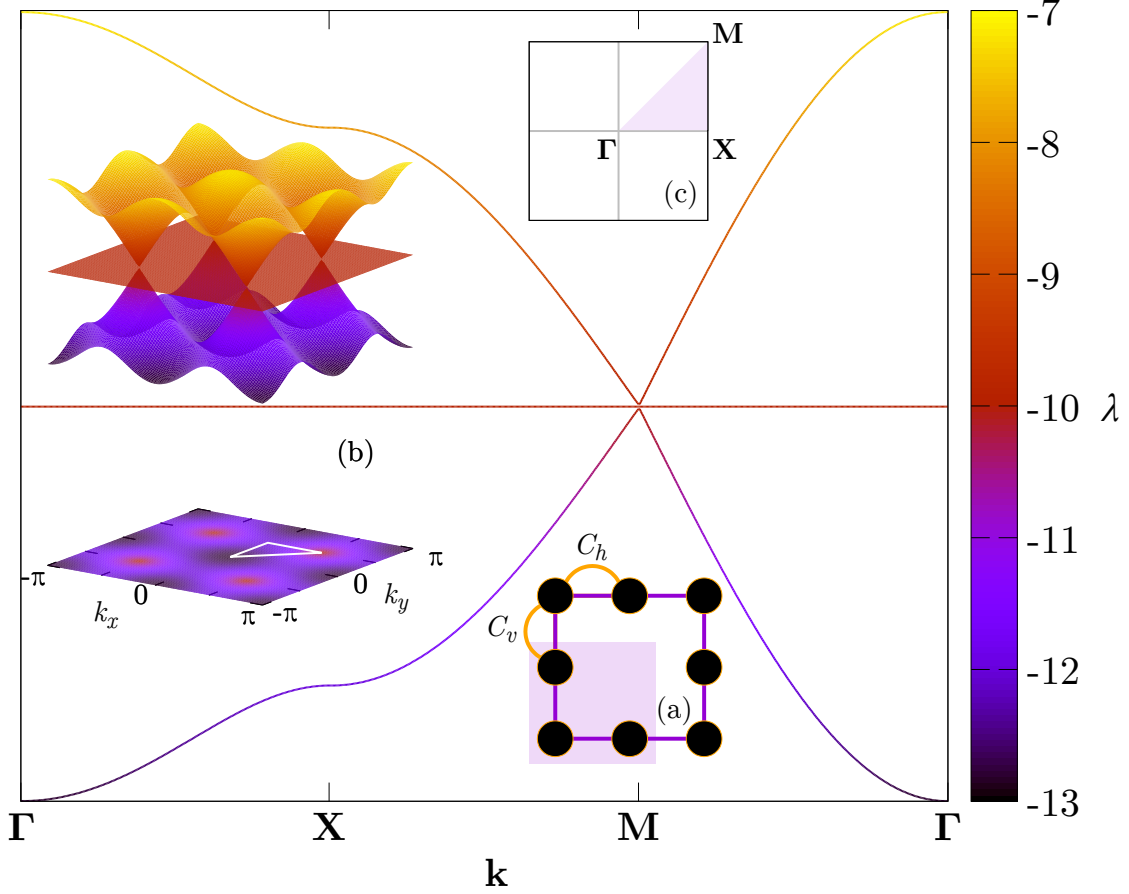


FIG. 1. Dispersion relation in the Lieb lattice for linear part of Eq. (1) along high symmetry points. Unitary cell of the lattice is represented with shadow region in (a). Irreducible Brillouin zone, corresponding to this unitary cell, is delimited with a white triangle in (b) and sketched in (c).

the Lieb lattice in the coupled mode approach becomes

$$\lambda = -\gamma, \quad \lambda_{\pm} = \pm 2\sqrt{C_h^2 \cos^2(k_x a) + C_v^2 \cos^2(k_y a)} - \gamma.$$

Hence, we can observe that there exist two conical interaction bands and one flat band, shown in Fig. 1 (b). These bands meet at single points, $\mathbf{M} = (\pm k_x n a, \pm k_y m a)$, called Dirac Points.

For the nonlinear case, we look for stationary solutions of model (1) of the usual form, $u_{n,m}(z) = \phi_{n,m} \exp(i\lambda z)$, where $\phi_{n,m}$ is the field amplitude which defines a complex spatial profile of the solution, and λ is the propagation constant. In this case we have a nonlinear

eigenvalue problem, given by

$$\lambda u_{\vec{n}} = \sum_{\vec{m}} C_{\vec{n},\vec{m}} u_{\vec{m}} - \gamma \frac{u_{\vec{n}}}{1 + |u_{\vec{n}}|^2}, \quad (2)$$

i. e., a set of coupled nonlinear complex algebraic equations. We are interested in solutions that have an integer number (S) of 2π phase changes in the azimuthal direction, so that, the phase profile twists in a helical manner as the beam propagates. In such a case, the self-localized solution is called a discrete vortex soliton, which have been predicted, both in conservative [16] and dissipative [17] system.

III. LOCALIZED VORTEX TYPE SOLUTIONS

As a particular setting for our analysis, we assume a focusing media by choosing a positive value for nonlinear coefficient ($\gamma = 10$). In order to find nonlinear VBs we proceed to solve Eq. (2) by implementing numerically a Newton-type algorithm. By choosing proper and reasonable seeds, in each case, and setting $C_v = C_h = 1$, we unveil families of stationary solutions with different values of TCs. In addition, we perform a standard linear stability analysis (see appendix in ref [18]) for the whole set of solutions. From now on we use solid (dashed) lines to denote family regions where VBs are stable (unstable).

We begin by presenting results of stationary vortex solitons with one TC ($S = 1$). Figure 2 shows the power content $P = \sum_{\vec{n}} |u_{\vec{n}}|^2$ vs λ diagrams corresponding with two different kind of localized modes. In both cases, their main spots are unfolded along an off-site place circuit: a square one for solutions belonging to the family represented by a green curve, and a ring one for those corresponding with magenta curve. Amplitude and phase spatial profiles, for both modes, are sketched in Fig. 2 (a1, a2) and Fig. 2 (b1, b2), respectively.

It is worth mentioning that modes belonging to the green curve exist for almost the entire λ domain: high power solutions are not restricted, and low-power ones exist for values close to the maximum value of the upper linear band, $\lambda = 2\sqrt{2} - \gamma$, at $\Gamma = (0, 0)$ point [cf. Fig. 1]. One reason for this behavior could be that spatial profile for this kind of mode can be seen as a superposition of four fundamental bright solitons, which bifurcate from the fundamental band-edge mode [19]. However, unlike the fundamental ones, here the phase distribution is not trivial. The four main spots are locked in a special manner, so, the solution does not bifurcate from the linear band and the green curve turns back at $\lambda \approx -7.04$. On the

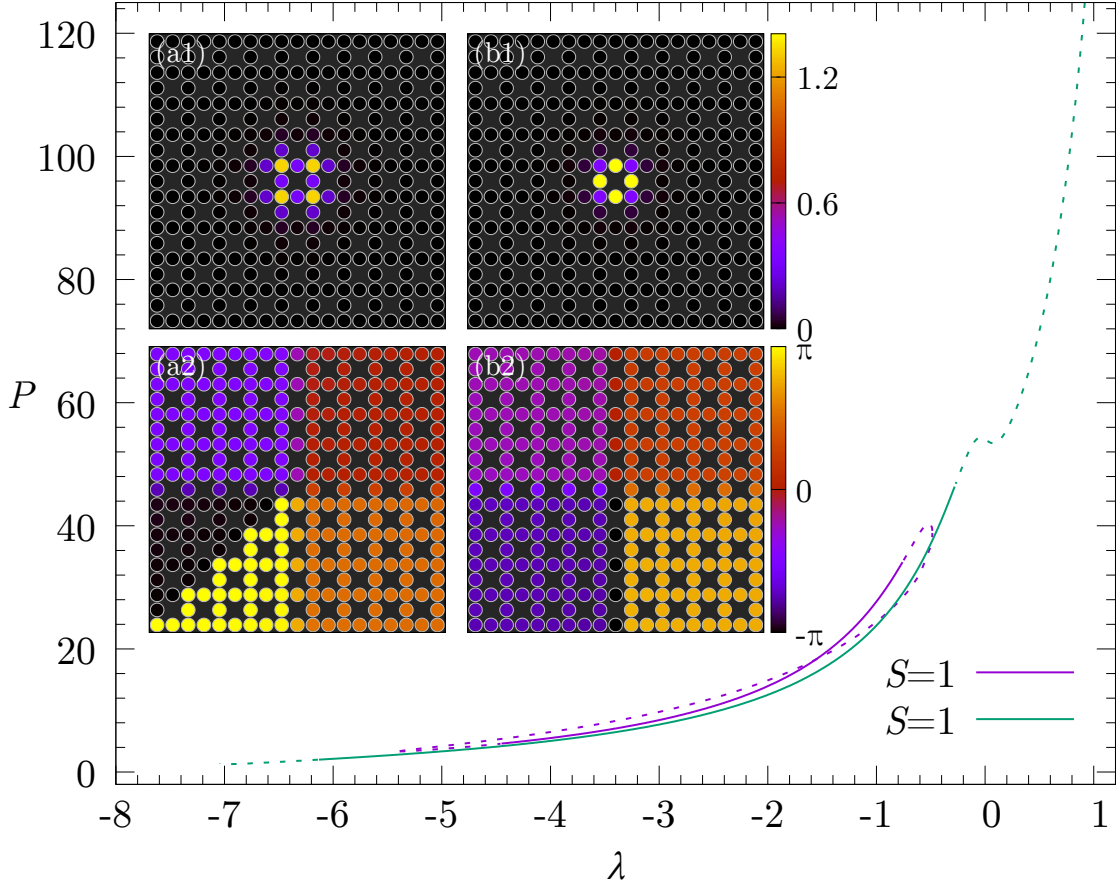


FIG. 2. P vs λ diagrams for two families of discrete vortex solitons with $S = 1$. Amplitude (a1, b1) and phase (a2, b2) profiles, at $\lambda = -3.0$, correspond to solutions belonging to the families represented by the green and magenta curve, respectively.

contrary, for the magenta curve, the lowest power value solution corresponds to $\lambda \approx -5.38$ where the family turns back increasing again its power up to $\lambda \approx -0.52$. From here, power decreases and the family turns back again. In general, both types of solutions destabilize for low and high power values (at least in our finite range of parameters), nevertheless, they span sizable stable regions. It is interesting to point out that there exist two different types of ring mode solutions with the same power at equal values of propagation constant ($\lambda \approx -1.55$), one stable and the other one unstable.

We focus now on the results of stationary vortex solitons with two TCs ($S = 2$). Figure 3 shows P vs λ diagrams corresponding with another pair of localized modes. For the present case, their main spots are unfolded along irregular hexagonal paths: a small one for solutions

belonging to the family represented by magenta curve, and a big one for those corresponding with green curve. Amplitude and phase spatial profiles, for both modes, are sketched in Fig. 3 (a1, a2) and Fig. 3 (b1, b2), respectively. It is important to point out that amplitude profiles for last modes do not resemble the $S = 1$ ones discussed at first, who had a smaller size. Instead, it should be emphasized that both of them look like asymmetric localized patterns vertically orientated.

The small hexagonal mode possesses two vertical edges with length equal to $2a$ and four diagonal edges with length equal to $\sqrt{2}a$ [Fig. 3 (a1)]. This kind of pattern can be presumed as the juxtaposition, along the vertical axes, of two ring modes [cf. Fig. 2(b1,b2)] properly oriented. The last one possesses two vertical edges with length also equal to $2a$ and four diagonal edges with length equal to $\sqrt{8}a$ [Fig. 3 (b1)]. On the other hand, the spatial phase profile for small hexagon mode [Fig. 3 (a2)] displays abrupt changes along closed paths around the centroid of the pattern. This behavior is not exclusive for periodical systems [20]. Even more, its variation does not occur continuously. Perhaps, that information is missing because the DNLS model does not account for any light propagating outside of the waveguides as evanescent waves. By contrast, the phase profile for the second mode [Fig. 3 (b2)] exhibits a smoothly variation. When power goes down the family represented by the green curve gets closer to the linear band and it turns back at $\lambda = -6.97$. The magenta curve behaves similarly, but it does not come so close to this band and its returning point is located at $\lambda = -6.23$.

Finally, we examine couple more cases of stationary vortex solitons with two and three TCs ($S = 2$ and $S = 3$), respectively. Figure 4 shows P vs λ diagrams corresponding with these two localized modes. In both cases, their main spots are unfolded along closed path trajectories: a hexagon one equivalent to that sketched at Fig. 3(a1,a2), for solutions belonging to the family represented by a green curve, and an octagon one for those being part of green curve. Amplitude and phase spatial profiles, for both modes, are sketched in Fig. 4 (a1, a2) and Fig. 4 (b1, b2), respectively. Despite hexagonal amplitude profiles depicted in Fig. 3(a1) and Fig. 4(a1) looks very similar, even with the same segment lengths, the number of lattice sites enclosed by those spatial trajectories are not the same. In this case, the juxtaposition would be between two on-site ring modes. Nevertheless, although the TC for both cases is the same, the spatial phase profile for the present case exhibits a smoothly variation. On the other side, modes with octagonal profile possesses two vertical and two

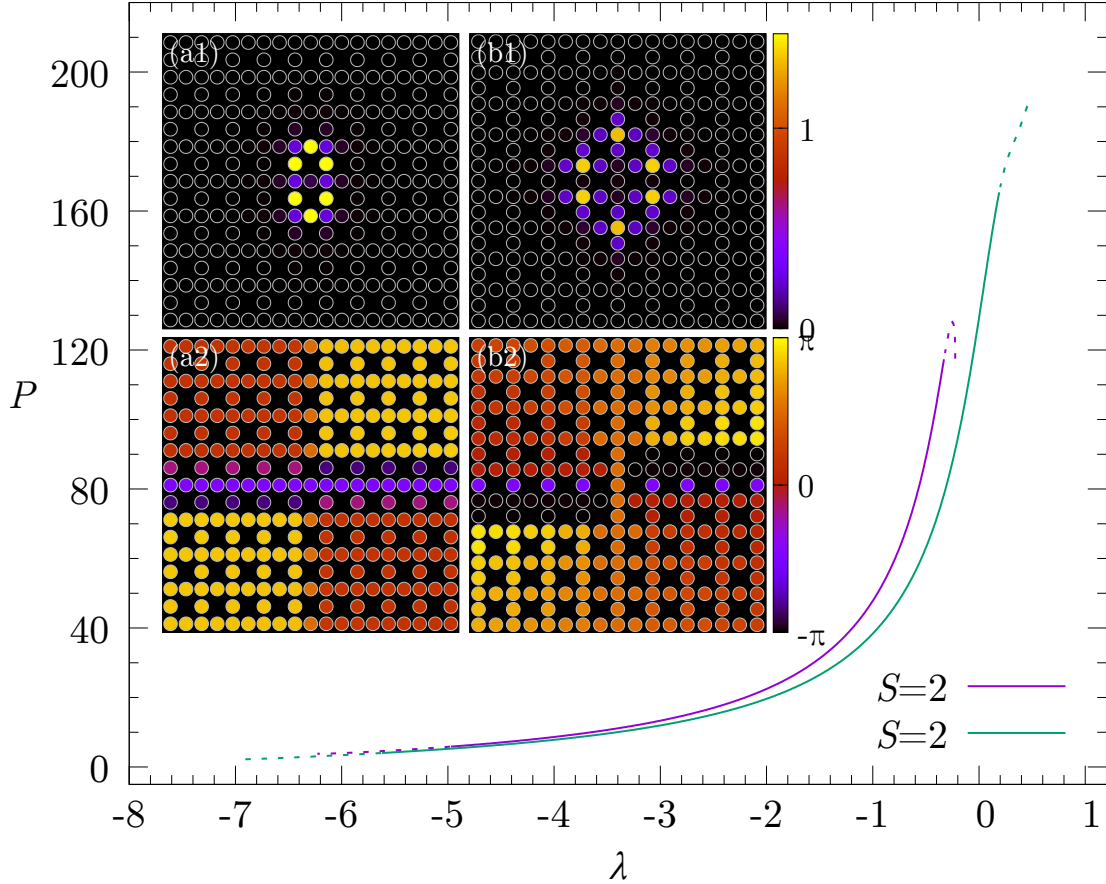


FIG. 3. P vs λ diagrams for two families of discrete vortex solitons with $S = 2$. Amplitude (a1, b1) and phase (a2, b2) profiles, at $\lambda = -3.0$, correspond to solutions belonging to the families represented by the green and magenta curve, respectively.

horizontal edges with length equal to $2a$ and four diagonal edges with length equal to $\sqrt{8}a$ [Fig. 4 (b1)]. Here again, phase profile also varies softly displaying clearly three TCs.

In general, we note that stable solutions with higher values of TCs, and a reasonably well-behaved phase variation, display a bigger spatial profile. Our results show that for vortex solitons with $S = 1$ their pattern are composed of four main spots, two less than those with $S = 2$ (hexagon). For the $S = 3$ case, their amplitude profile exhibit eight main spots (octagon) two more than previous one. Apparently, as many peaks are present in the amplitude profile the solutions can endow a higher value of TC. This approach looks like effective to find VBs with TC greater than $S = 3$. However, and after following this insight, we could not find solutions with this attribute. It seems that the highest allowed value for

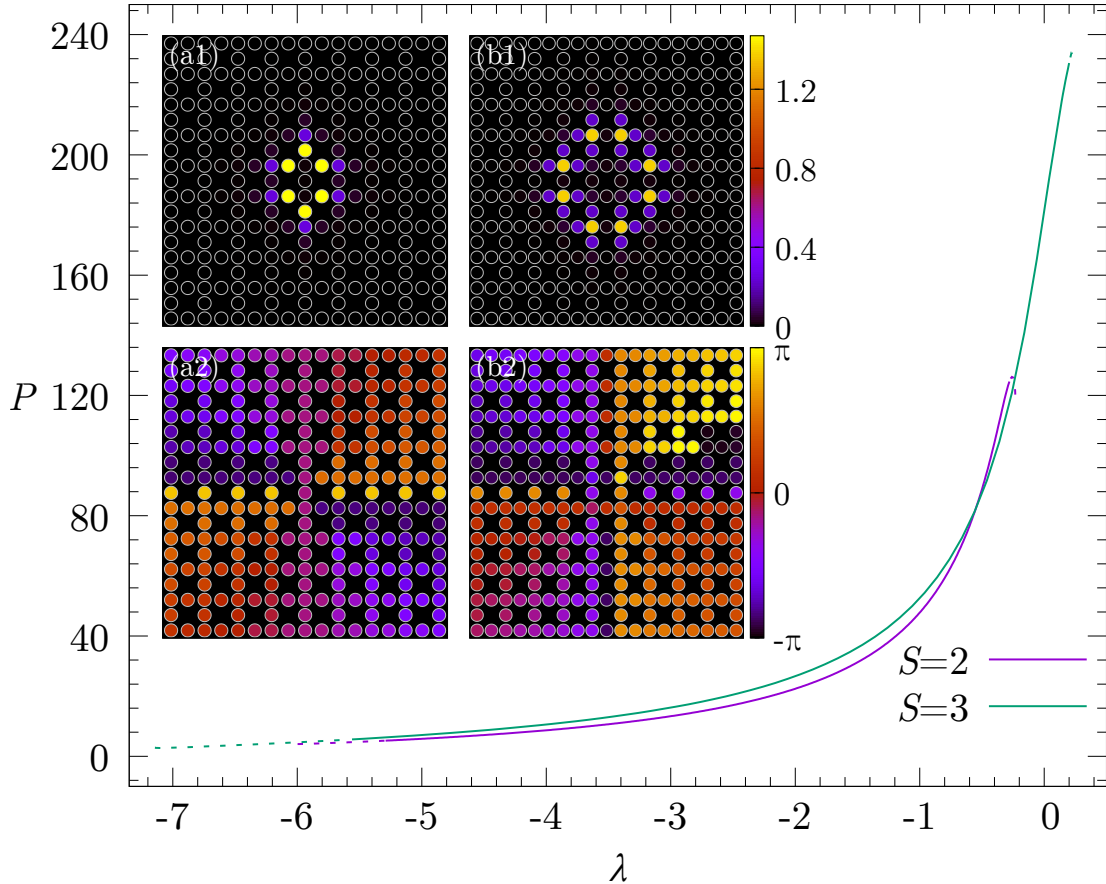


FIG. 4. P vs λ diagrams for two families of discrete vortex solitons with $S = 2$ (magenta) and $S = 3$ (green). Amplitude (a1, b1) and phase (a2, b2) profiles, at $\lambda = -3.0$, correspond to solutions belonging to these families represented by the green and magenta curve, respectively.

the TC is restricted by the order of discrete point-symmetry group of the lattice [21].

IV. STABILITY AGAINST ANISOTROPY

So far, we have analyzed the existence and stability of localized nonlinear vortex modes with different TCs in terms of P vs λ diagrams. Having in mind the anisotropic constraint, imposed by the photorefractive effect [22], in a hypothetical experimental realization of these kind of lattices, we extended our analysis to the anisotropic case ($C_v \neq C_h$). By adding this quantity as a new parameter in our workspace, we could figure out how reasonable would be the experimental observation of this kind of localized patterns. To do that, we must first unveil the existence domain, for one specific type of localized vortex solution, as a function

of the λ and C_v parameters. That is, we must make sure that the whole set of solutions in (λ, C_v) domain feature the same characteristics, namely, TC and spatial amplitude distribution. In general, we have observed that anisotropy shrinks P vs λ diagrams, both in existence and stability. Therefore, starting from the isotropic case, and by increasing adiabatically the strength of anisotropy, we explore a region of parameters to identify cartesian boundaries of a (λ, C_v) subspace. Once this has been outlined, we perform a detailed scan of its inside. Figure 5 displays the stability diagrams for vortex modes reported above in terms of the anisotropy of the system. The size of (λ, C_v) subspace is $\{\lambda_1, \dots, \lambda_N\} \times \{C_{v_1}, \dots, C_{v_N}\}$ being $N = 100$, i. e., each one of these plots are sampled with 10^4 points, where each point corresponds to one specific stationary solution.

For ring modes with $S = 1$ we can appreciate from Fig. 5(a) a considerable inner region where this kind of solution remains stable. Depending of the λ value, a higher strength of anisotropy can be supported for these kind of vortices, finding that maximum value allowed here for anisotropy is $C_v \simeq 1.40$ at $\lambda \simeq -2.14$. A really different behavior occurs when we analyze the stability properties of square modes with $S = 1$. From Fig. 5(b) we note that the stable region is almost imperceptible; once we move along the anisotropy axis, the solutions becomes unstable except for $\lambda \simeq -0.56$, where a narrow stability window raises up to a strength anisotropy value of $C_v \simeq 1.25$. We turn now to stability regions for modes with two TCs ($S = 2$) and asymmetric hexagonal profiles. In the first case, for those modes displayed at Fig. 3(a1,a2), we observe that strength of anisotropy allowed for the off-site hexagon [Fig. 5(c)] is $C_v \simeq 1.66$ corresponding to $\lambda \simeq -1.88$. Next case, for those modes displayed at Fig. 3(b1,b2), they also possesses a stable region but smaller than the previous case with maximum value for anisotropy $C_v \simeq 1.34$ at $\lambda \simeq -0.9$. In the last case, pertaining to the modes depicted at Fig. 4(a1,a2), even when the existence domain is smaller than for the first case their stable regions are very similar. Finally, we scrutinize the stability region for modes endowed with three TCs ($S = 3$), and an octagonal amplitude profile as those represented in Fig. 4(b1,b2). Here, we also observe [cf. Fig. 5] a sizeable stable region where stable vortex can support anisotropic values up to $C_v = 1.6$ at $\lambda \simeq -0.68$.

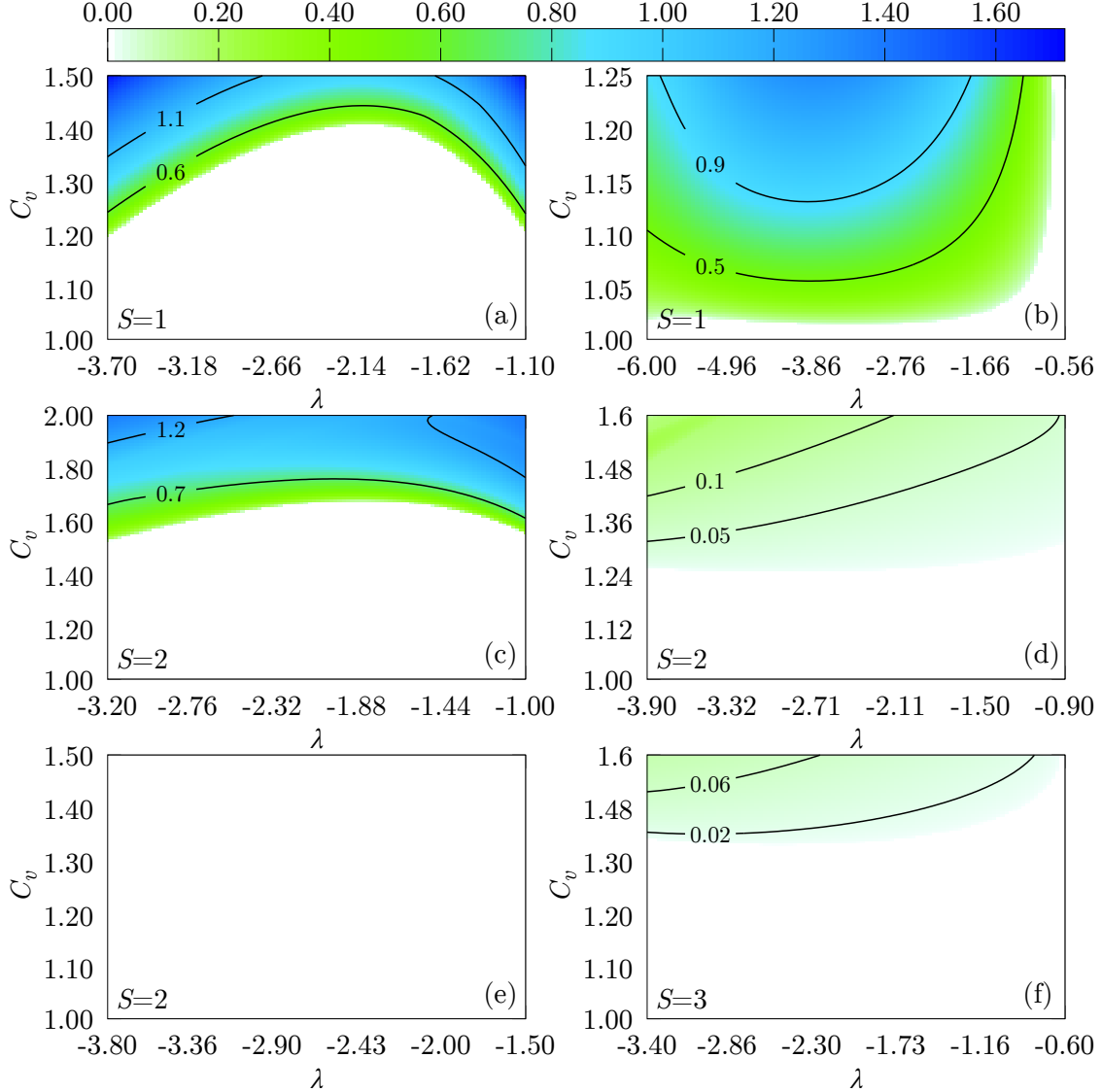


FIG. 5. Colormap plots for stability domains as function of λ and C_v for diverse vortex solitons. Modes endowed with one TC: (a) ring amplitude profiles and (b) square amplitude profiles. Modes endowed with two TC with three different (c)-(e) asymmetric hexagonal amplitude profiles. Mode with (f) octagonal profile and three TCs.

V. CONCLUSIONS

Recapitulating, we have analyzed the existence and stability of VBs with diverse values of TCs, in periodic media with saturable nonlinearity, as function of parameters of the system. Families of stationary solutions with one, two and three topological charges has been unveiled. In general, as we enforce our model to obtain vortices with TCs greater than

$S = 1$, the number of main spots increases, what leads to spatial amplitude profiles become larger. On the other hand, by studying the role played in the system by the presence of anisotropy, we identify domains of stability for each type of mode reported here. We showed that those vortices that could be regarded as generated from two ring modes, display larger stable regions than others.

We consider that model employed along this work might fit pretty well for waveguide arrays imprinted in photorefractive crystals, therefore, we hope that our findings stimulate fabrication for these photonic lattices, and additionally they pave the way for the observation of these VBs.

Acknowledgments: Powered@NLHPC: This research was partially supported by the supercomputing infrastructure of the NLHPC (ECM-02). M. I. M. acknowledges support from Fondecyt grant 1160177.

Disclosures: The authors declare no conflicts of interest.

-
- [1] G. Molina-Terriza, J. P. Torres, and L. Torner, *Phys. Rev. Lett.* **88**, 013601 (2001).
 - [2] A. Mair, A. Vaziri, G. Weihs, and A. Zeilinger, *Nature* **412**, 313 (2001).
 - [3] X. Zhuang, *Science* **305**, 188 (2004), <https://science.sciencemag.org/content/305/5681/188.full.pdf>.
 - [4] I. A. Favre-Bulle, A. B. Stilgoe, E. K. Scott, and H. Rubinsztein-Dunlop, *Nanophotonics* **8**, 1023 (2019).
 - [5] J. T. Barreiro, T.-C. Wei, and P. G. Kwiat, *Nature Physics* **4**, 282 (2008).
 - [6] S. D. Ganchev, E. L. Ivchenko, S. N. Danilov, J. Eroms, W. Wegscheider, D. Weiss, and W. Prettl, *Phys. Rev. Lett.* **86**, 4358 (2001).
 - [7] P. L. Kelley, *Phys. Rev. Lett.* **15**, 1005 (1965).
 - [8] Y. V. Kartashov, C. Hang, G. Huang, and L. Torner, *Optica* **3**, 1048 (2016).
 - [9] T. J. Alexander, A. A. Sukhorukov, and Y. S. Kivshar, *Phys. Rev. Lett.* **93**, 063901 (2004).
 - [10] D. N. Neshev, T. J. Alexander, E. A. Ostrovskaya, Y. S. Kivshar, H. Martin, I. Makasyuk, and Z. Chen, *Phys. Rev. Lett.* **92**, 123903 (2004).
 - [11] J. Armijo, R. Allio, and C. Mejía-Cortés, *Opt. Express* **22**, 20574 (2014).
 - [12] A. Szameit and S. Nolte, *Journal of Physics B: Atomic, Molecular and Optical Physics* **43**, 163001 (2010).

- [13] G. R. Castillo, L. Labrador-Páez, F. Chen, S. Camacho-López, and J. R. V. de Aldana, *J. Lightwave Technol.* **35**, 2520 (2017).
- [14] R. A. Vicencio, C. Cantillano, L. Morales-Inostroza, B. Real, C. Mejía-Cortés, S. Weimann, A. Szameit, and M. I. Molina, *Phys. Rev. Lett.* **114**, 245503 (2015).
- [15] S. Mukherjee, A. Spracklen, D. Choudhury, N. Goldman, P. Öhberg, E. Andersson, and R. R. Thomson, *Phys. Rev. Lett.* **114**, 245504 (2015).
- [16] B. A. Malomed and P. G. Kevrekidis, *Phys. Rev. E* **64**, 026601 (2001).
- [17] C. Mejía-Cortés, J. M. Soto-Crespo, R. A. Vicencio, and M. I. Molina, *Phys. Rev. A* **83**, 043837 (2011).
- [18] C. Mejía-Cortés, J. M. Soto-Crespo, R. A. Vicencio, and M. I. Molina, *Phys. Rev. A* **86**, 023834 (2012).
- [19] B. Real and R. A. Vicencio, *Phys. Rev. A* **98**, 053845 (2018).
- [20] J. Soto-Crespo, N. Akhmediev, C. Mejía-Cortés, and N. Devine, *Opt. Express* **17**, 4236 (2009).
- [21] Y. V. Kartashov, A. Ferrando, A. A. Egorov, and L. Torner, *Phys. Rev. Lett.* **95**, 123902 (2005).
- [22] B. Terhalle, A. S. Desyatnikov, C. Bersch, D. Träger, L. Tang, J. Imbrock, Y. S. Kivshar, and C. Denz, *Applied Physics B* **86**, 399 (2007).